*Molecular Vision* 2015; 21:538-547 <http://www.molvis.org/molvis/v21/538>
Received 11 February 2015 | Accepted 30 April 2015 | Published 2 May 2015



# Third harmonic generation microscopy of a mouse retina

**Omid Masihzadeh,[1] Tim C. Lei,[2] Scott R. Domingue,[3] Malik Y. Kahook,[1] Randy A. Bartels,[3] David A. Ammar[1]**

*[1]Department of Ophthalmology, University of Colorado Denver, Aurora, CO; [2]Department of Electrical Engineering, University of Colorado Denver, Denver, CO; [3]Department of Electrical Engineering, Colorado State University, Fort Collins, CO*

**Purpose:** To demonstrate lipid-specific imaging of the retina through the use of third harmonic generation (THG), a multiphoton microscopic technique in which tissue contrast is generated from optical inhomogeneities.
**Methods:** A custom fiber laser and multiphoton microscope was constructed and optimized for simultaneous two-photon autofluorescence (TPAF) and THG retinal imaging. Imaging was performed using fixed-frozen sections of mouse eyes without the use of exogenous fluorescent dyes. In parallel experiments, a fluorescent nuclear stain was used to verify the location of the retinal cell nuclei.
**Results:** Simultaneous THG and TPAF images revealed all retinal layers with subcellular resolution. In BALB/c strains, the THG signal stems from the lipidic organelles of the cellular and nuclear membranes. In the C57BL/6 strain, the THG signal from the RPE cells originates from the pigmented granules.
**Conclusions:** THG microscopy can be used to image structures of the mouse retina using contrast inherent to the tissue and without the use of a fluorescent dye or exogenously expressed recombinant protein.

Advances in optical coherence tomography (OCT) [1-3] and adaptive optics [4-6] within the last few decades have revolutionized the way we image the retina. Despite impressive developments in these label-free linear imaging technologies, a wide array of pathological changes cannot be visualized in patients or animals with retinal diseases. This lack of functional imaging arises from deficiencies in two main areas: an absence of subcellular resolution and a lack of molecular-specific contrast. Here, we show a non-invasive, label-free retinal imaging technique based on third harmonic generation (THG) [7,8], a multiphoton microscopic technique in which the contrast arises from optical inhomogeneities that are comparable in size to the beam focus. In biologic tissues, for example, THG microscopy produces three-dimensional images in which the contrast originates from the interface between an aqueous and cellular membrane [9], lipid droplets and lipidic organelles [10-12], or highly absorptive molecules. For example, Aptel et al. have shown THG images of the cornea epithelium that originate from the cell and nuclear boundaries [13].

In this paper, we successfully used simultaneous two-photon autofluorescence (TPAF) [14] and THG to image cross sections of full-thickness mouse retinas with subcellular resolution. The third harmonic contrast arises from the lipid-rich cell membranes surrounding the cytoplasm and the cell nuclei as well as pigments in the RPE cells. We used a laser scanning technique to acquire images across the entire retina and identified all cellular layers including the RPE, outer and inner nuclear layers, and ganglion cells. The images collected with TPAF/THG are on par with those imaged with light microscopy from adjacent histological sections. We believe THG microscopy can lead to a tool for functional imaging of the retina and be used to generate virtual cross sections of intact eyes without the need for standard tissue processing techniques.

Correspondence to: Omid Masihzadeh, Department of Ophthalmology, University of Colorado School of Medicine, 12800 E 19th Ave, MS 8311, RC-1 North Room #5115, Aurora, CO, 80045; Phone: (303) 724-6958; FAX: (303) 724-5270; email: Omid.Masihzadeh@UCDenver.edu.

## METHODS

*Sample preparation of mouse eye tissue:* This research was conducted in compliance with the ARVO Statement for the Use of Animals in Ophthalmic and Vision Research. All mice were handled in strict accordance with good animal practice, and all animal work was approved by the Institutional Animal Care and Use Committee at the University of Colorado Anschutz Medical Campus (Aurora, CO). Eyes from the C57BL/6 strain were obtained from Jackson Labs (Bar Harbor, ME). Mice from the BALB/c strain (Harlan Laboratories, Indianapolis, IN) were provided by the Office of Laboratory Animal Resources (University of Colorado, Denver). All mice were between 4 and 6 months of age. After the animals were euthanized by $CO_2$ inhalation, the eyes were enucleated, placed in Davidson's Fixative (33% ethanol, 11% glacial acetic acid, 8% formaldehyde) for 4 h, and then flash-frozen in optimum cutting temperature (Tissue-Tek OCT; Sakura Finetek USA Inc., Torrance, CA). Eyes were cut into 20 µm thick sections, washed in PBS (137 mM sodium chloride, 2.7 mM potassium chloride, 1.5 mM potassium

phosphate monobasic, 8.1 mM sodium phosphate dibasic, pH 7.4), and then mounted in PBS for THG/TPAF imaging. In some experiments, the tissue sections were incubated for 5 min in 2 µM ethidium homodimer-1 (EthD-1; Life Technologies, Grand Island, NY) before imaging.

*Cell culture:* Opossum kidney (OK) cells were a gift from Dr. Moshe Levi (UC Denver). Cells were grown on glass coverslips in Dulbecco's modified Eagle's media (Life Technologies) supplemented with 10% fetal calf serum (FBS; Life Technologies). Human fetal RPE (hfRPE) cultures were a gift from Dr. Sheldon Miller (National Eye Institute, NIH). The hfRPE cells were grown on Transwell filters (Corning Costar, Corning, NY) coated with human extracellular matrix (BD Biosciences, Franklin Lakes, NJ) in minimum essential media (alpha modification; Sigma Aldrich, St. Louis, MO) supplemented with N1 supplement (Sigma), glutamine-penicillin-streptomycin G (Sigma), non-essential amino acids (Sigma), 250 mg/l taurine (Sigma), 20 µg/l hydrocortisone, (Sigma), 0.013 µg/l triiodothyronine (T3 hormone; Sigma), and 5% FBS [15]. Cells were fixed with Davidson's Fixative for 20 min, rinsed three times in PBS, and mounted in PBS for THG/TPAF imaging.

*Histologic staining and photography:* The sections adjacent to the THG/TPAF sections were stained with Mayer's hematoxylin and eosin Y (H&E; Richard-Allan Scientific, Kalamazoo, MI). Bright-field imaging of mouse histological sections was performed with a Nikon Eclipse 80i microscope (Melville, NY) equipped with a color camera (D5-Fi1; Nikon) and a 20X Plan Fluor objective lens (Nikon).

*Imaging platform:* The retina images were acquired with a custom-built multiphoton microscope platform optimized for simultaneous THG and TPAF imaging (Figure 1A). The laser system was a custom-built all-normal-dispersion femtosecond fiber laser [16] generating 600 mW of 1044 nm femtosecond pulses with a repetition rate of 63 MHz. The laser pulses were pre-compressed to about 200 fs at the sample. Raster scanning of the laser focus across the sample was achieved with two non-resonant galvanometric mirrors (6220HM60B; Cambridge Technology, Watertown, MA). The pulse train with an average power of 8 mW (incident at the sample) was focused with an Olympus UPlanSApo 60X/1.2 NA water objective (Olympus). Due to the small scanning mirrors (5-mm clear aperture), the focusing objective was well underfilled resulting in a decrease in the effective numerical aperture from 1.2 to 0.7. Imaging was performed on a custom-built upright microscope equipped with two single-photon counting photomultiplier tubes (PMTs) detectors; one in the epidetection (backward direction) collected TPAF signal through the focusing objective lens, and the other in the forward direction collected the THG signal with a custom-built compound collection lens with an NA of 0.9. A dichroic mirror (FF705-Di01, Semrock, Rochester, NY) and a bandpass filter (HQ550/100 M-2p, Chroma Technology Corp, Bellows Falls, VT; transmission from 500 to 600 nm signal) were used in the epidetection to separate the TPAF from the incident excitation beam. Note that the large transmission window of the TPAF bandpass filter would allow for detection of any second harmonic (SH) signal generated by the sample. However, due to the lack of collagen in the retina, we did not expect any SH signal [17]. The forward THG signal was filtered with a second dichroic mirror (FF409-Di03, Semrock, Rochester, NY) and a bandpass filter (FF01–390/SP-25, Semrock).

*Image analysis and processing:* A custom software package written in Visual C# was used to collect all images. Acquired images were post-processed for background noise reduction and prepared in their current format with ImageJ software. Images shown here are representative of 15 experiments on BALB/c mice and five experiments on C57BL/6J mice.

## RESULTS

The image in Figure 1E demonstrates the THG signal (red) from the lipid-rich nuclear membrane (+), cell membrane (*), and lipid droplets (x) of an opossum kidney cell creates a biomarker for lipid-specific functional microscopy. OK cells were used since these cells have been shown to accumulate intracellular lipid droplets [18]. Figure 1F shows that the pigment granules (x) of a cultured hfRPE cell also generate a THG signal.

Sagittal and transverse sections of the full-thickness mouse retina were imaged perpendicular to the surface (Figure 2). Simultaneous THG (red) and TPAF (green) images of the retina show a low degree of colocalization of the two signals that manifest from the distinct imaging contrast between the two modalities. The cellular and extracellular material emitted a strong TPAF signal, likely due to the aromatic amino acids within the proteins. Due to the wide (100 nm) emission filter used in the experiment, the exact source of autofluorescence (AF) is undefined. Generally, four regions of the retina consistently emitted TPAF: the inner and outer plexiform layers and the inner and outer photoreceptor segments. Fluorescent adducts from formaldehyde fixation accounted for some of this AF [19]; however, in experiments that used unfixed retinal tissue, the TPAF signals were decreased but qualitatively the same (data not shown).

As shown in Figure 2A and 2E, all cell layers of the retina were resolved. A layer of cells at the inner boundary of the retina (bottom of Figure 2A) was apparent (Figure 2D,

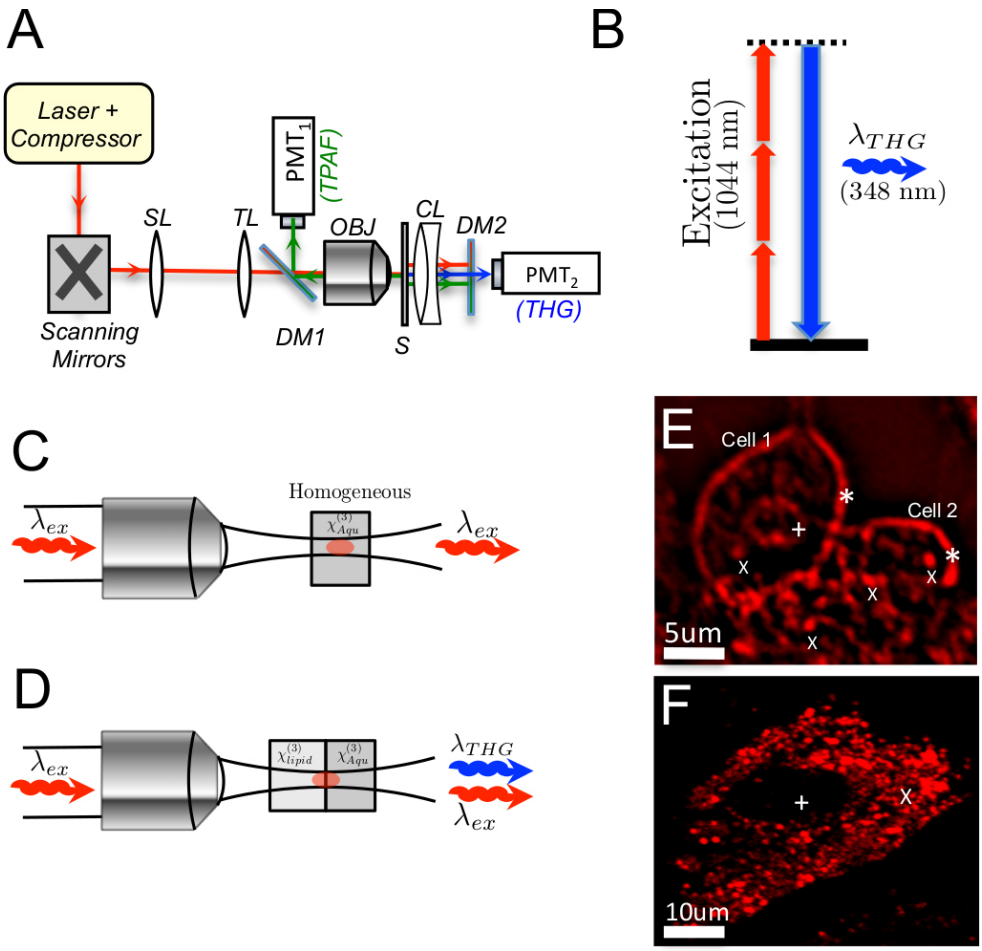


Figure 1. Multiphoton microscopy setup for simultaneous third harmonic generation (THG) and two-photon autofluorescence (TPAF) imaging of retina. **A**: A femtosecond fiber laser oscillator generates a 1044-nm laser beam to target the cross sections of full-thickness mouse retina. The laser beam is scanned and focused across the sample with a 60X microscope objective (OBJ). A dichroic mirror (DM1) separates the excitation laser beam (1044 nm) from the TPAF signal (522 to 600 nm) traveling in the backward (epi) direction and detected with a photomultiplier ($PMT_1$). A high numerical aperture condenser lens (CL) collects the forward propagating THG signal. A second dichroic mirror and a narrow band filter sets separate the forward propagating TPAF and excitation beams from the THG signal (348 nm), which is detected with a photomultiplier ($PMT_2$), DM1: dichroic mirror, SL: scanning lens, TL: tube lens, OBJ: objective, S: sample, CL: condenser lens, DM2: dichroic and narrow band filter, PMT: photomultiplier. **B**: A Jablonski diagram showing the interaction of multiple infrared photons between the electronic ground state and the electronic virtual state. In THG, three infrared excitation photons are instantaneously up-converted into a single photon of three times the energy. **C**: Under multiphoton microscopic conditions, no THG signal is generated inside a homogenous medium, i.e., the aqueous media of the cytoplasm. **D**: At the interface of two media with different nonlinear susceptibilities, i.e., the aqueous media and the lipidic organelle, significant THG is generated at the focus of the excitation beam. **E**: The THG signal from the lipid-rich nuclear membrane (+), cell membrane (*), and lipid droplets (x) of an opossum kidney (OK) cell create a biomarker for lipid-specific functional microscopy. **F**: THG signal from the pigment granules (x) of a cultured human fetal RPE (hfRPE) cell. The region with no THG signal (+) represents the nuclei.

+), and based on the position, size, and DNA staining, we concluded that these were the cells of the ganglion cell layer (GCL). Adjacent to the GCL was a 50-µm-thick region, the inner plexiform layer (IPL), which predominantly emitted TPAF along with a weak, punctate THG signal (Figure 2A). Above the IPL, a multinuclear layer (eight to ten nuclei) was observed in the THG channel (Figure 2A inset and 2C, x). This region is approximately 40 µm thick, corresponding to the inner nuclear layer (INL). Following the INL is the thin 15-µm-thick outer-plexiform layer (OPL). Similar to the IPL, the OPL emitted a strong AF with weak punctate THG signals. We recognized the multinuclei photoreceptor cell layer, the outer nuclear layer (ONL), through the strong THG signal from the photoreceptor nuclei membrane (Figure 2B,*). The ONL appears 12–14 nuclei deep and is approximately 50 µm thick. The regions of the photoreceptor segments, the inner segment (IS) and outer segment (OS), are also resolved in Figure 2B (the RPE layer is detached). The IS region emitted little TPAF while the OS region exhibited a strong TPAF signal and a punctate THG signal (Figure 2B). Due to the resolution of the microscope, the origin of these structures is unknown. Finally, a single layer of RPE cells with strong THG from the nuclear membranes is visible in Figure 2A (*). We attribute the strong TPAF signal to the intracellular retinoids. The experimental results for the pigmented mouse strain (C57BL/6J) are shown in Figure 2E. The most

noticeable difference here was the source of the THG signal predominantly from the pigment granules in the RPE cells (+).

Figure 3, Figure 4, and Figure 5 show the regions of the retina imaged with THG and TPAF with and without a fluorescent nuclear dye (EthD-1) counterstain alongside an adjacent histological section stained with hematoxylin and eosin. When the outer retina of the albino mouse eye is examined (Figure 3), the ONL shows strong THG from the nuclear membrane with no THG within the photoreceptor nuclei (Figure 3A), which are apparent in an adjacent section of the retina containing nuclear dye (Figure 3B). The fluorescently labeled photoreceptor nuclei emit a bright fluorescent (green) signal that does not overlap the THG signal (Figure 3B). In Figure 3C, the corresponding histological section shows the characteristic mature rod nuclei, with tightly packed heterochromatin stained intensely blue by hematoxylin. In the inner and outer segment region, the difference in light/dark eosin staining (Figure 3C) shows that the outer

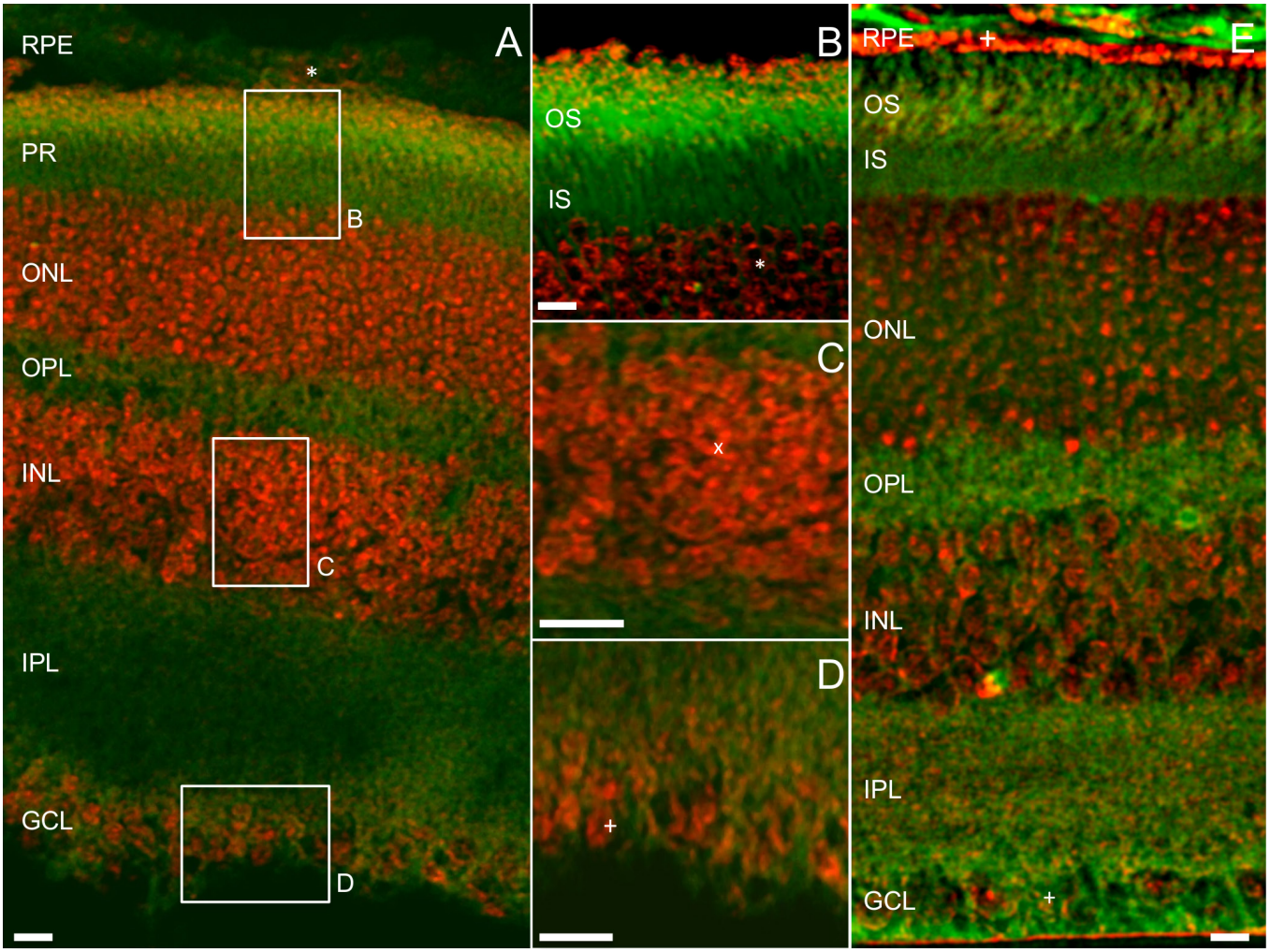


Figure 2. Multiphoton images of the mouse retina, with the THG signal shown in red and the TPAF signal shown in green. **A**: A sagittal/transverse retinal section of an albino (BALB/c) mouse eye, showing simultaneous third harmonic generation (THG) and two-photon autofluorescence (TPAF) signals from different layers of the retina. A significant THG signal is detected in the RPE layer, outer nuclear layer (ONL), inner nuclear layer (INL), and ganglion cell layer (GCL). The TPAF signal is predominantly generated at the photoreceptors (PRs), the outer plexiform layer (OPL), and the inner plexiform layer (IPL). **B**: The outer segment (OS), inner segment (IS), and cell nuclei (*) of the photoreceptors are resolved with THG (the RPE layer detached during processing). **C**: Individual cellular nuclear membrane (x) of the INL resolved with THG. **D**: Individual cellular nuclear membrane (x) of the ganglion cells resolved with THG. **E**: A sagittal/transverse retina section from a pigmented (C56BL/6) mouse eye. A strong THG signal originates from the pigment granules (+) within the RPE of the pigmented mouse sections, a signal not seen from the RPE layer within the albino sections in Panels **A** and **B**. Post-processing filters were applied for better visualization of the TPAF signal, which we believe are the photoreceptor cytoplasmic material or axons. Scale bar=10 µm.

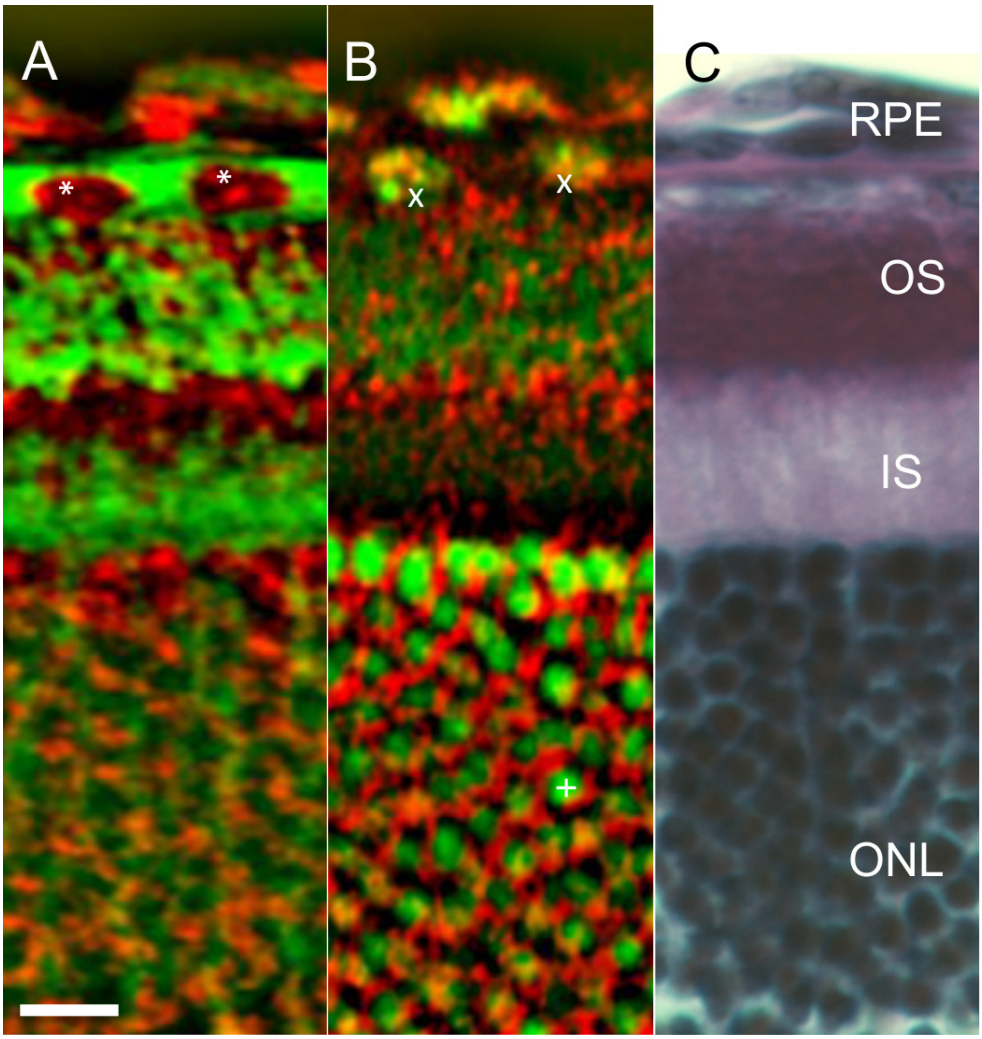


Figure 3. Comparison of the outer regions of the retina. **A**: Without a fluorescent nuclear dye (ethidium bromide homodimer; EthD-1) counterstain. **B**: With nuclear fluorescent dye. Panels **A** and **B** show the outer retina imaged with third harmonic generation (THG) and two-photon autofluorescence (TPAF). In the RPE layer, the EthD-1 staining (Panel **B**, x) coincides with the THG signal from the RPE cell nuclei (Panel **A**, *). In the outer nuclear layer (ONL), no THG signal is apparent in Panel **A** in the cell nuclei labeled with nuclear dye (Panel **B**, +). Here, the THG signal labels the ONL cell membrane. Panel **C** shows an adjacent histological section stained with hematoxylin and eosin. Scale bar=20 µm.

segments contain a large degree of tightly-packed protein and lipid disks compared to the inner segments. This difference was detected in the increase in the TPAF signal in the outer segments (Figure 3A,B). The outer segment discs appear to generate a diffuse THG signal. The source of this signal was not completely elucidated but could be due to the lipids inside the disk membrane that were not resolved.

In contrast to the photoreceptor nuclei that exhibited no THG signal, the nuclei of the RPE layer generated a significant THG signal, demonstrated by the overlap of the EthD-1 fluorescence (Figure 3B, x) and the THG (red, *) in Figure 3A. The THG signal from the nuclei of the RPE cells is qualitatively similar to the hematoxylin staining of the RPE nuclei (Figure 3C), which shows a pattern of dark and light blue due to the mixture of hetero- and euchromatin.

A similar pattern is seen in the inner retinal layers when images from label-free THG microscopy (Figure 4A and Figure 5A), EthD-1 counter stain (Figure 4B and Figure 5B), and histologically stained sections (Figure 4C and Figure 5C) are compared. The nuclei of the inner nuclear and ganglion cell layers have a punctate pattern (dark spots) under hematoxylin staining that likely corresponds to the contrast in the THG signal in these cell nuclei. The IPL and the OPL appear uniform with eosin staining (Figure 4C and Figure 5C), and both layers give a uniform TPAF signal (Figure 4A and Figure 5A). There is a faint pattern in the THG signal in the IPL and the OPL; however, the source of this signal was not apparent.

## DISCUSSION

Multiphoton imaging using lipids as biomarkers has been extensively applied to visualize biologic processes such as lipogenesis [20], intracellular trafficking of lipids and proteins [21] as well as how cultured cells interact with

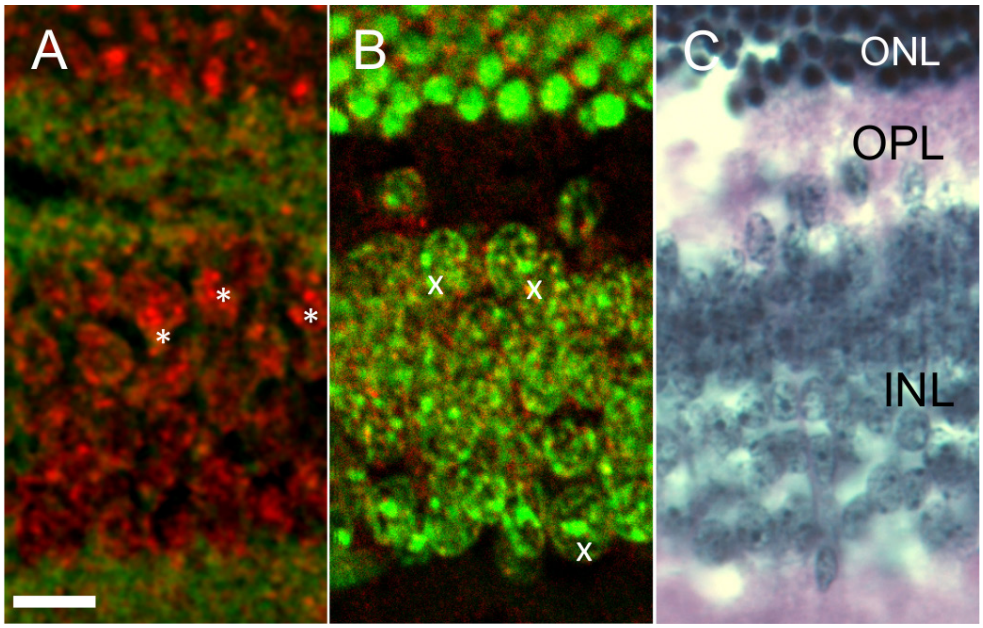


Figure 4. Comparison of the inner and outer nuclear layers of the retina. **A**: Without a fluorescent nuclear dye (ethidium bromide homodimer; EthD-1) counterstain. **B**: With nuclear fluorescent dye. Panels **A** and **B** show the inner nuclear layer imaged with third harmonic generation (THG) and two-photon autofluorescence (TPAF). The EthD-1 nuclear staining (Panel **B**, x), coincides with the THG signal from the cell nuclei (Panel **A**, *). **C**: An adjacent histological section stained with hematoxylin and eosin. Scale bar=20 µm.

three-dimensional scaffolds [22-24]. Recently, application of coherent anti-Stokes Raman scattering (CARS) [25-28] for non-invasive and label-free retinal imaging [29] was demonstrated by our group. Here, vibrations of lipid molecules within the cell membrane of photoreceptors and the RPE formed the contrast for imaging the photoreceptor outer segments of an intact mouse eye. CARS microscopy requires two optical wavelengths (pump and Stokes lasers) to arrive simultaneously at the samples to excite the vibrations of lipid molecules. The application of CARS for in vivo retinal imaging, which requires spatial and temporal overlap of the two optical pulses at the sample, demands complicated optical

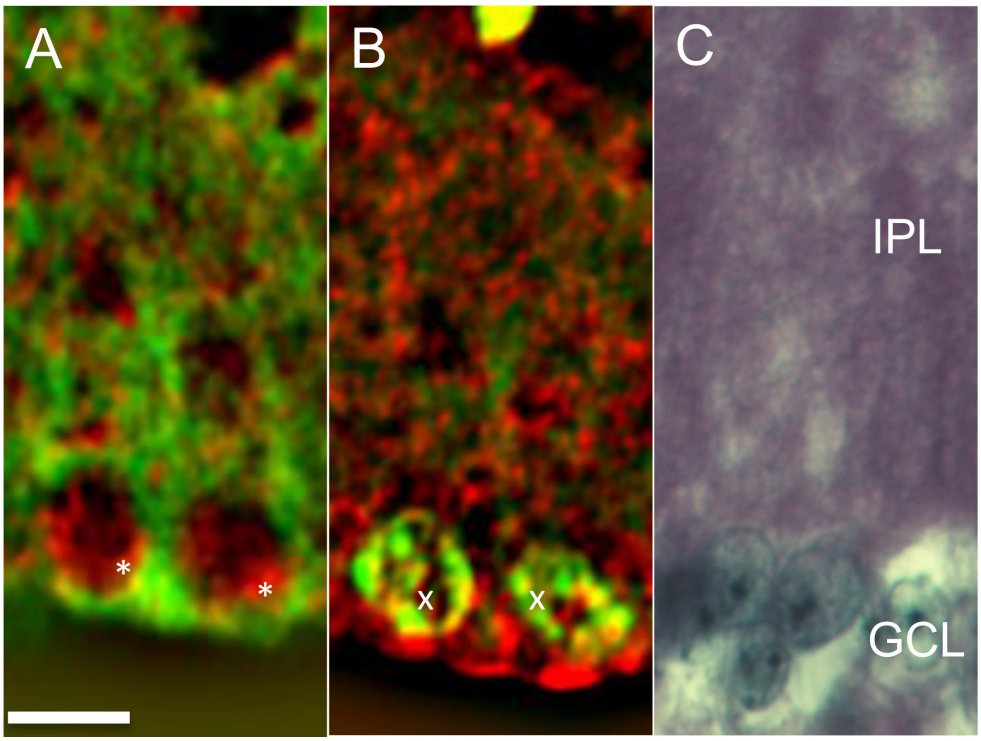


Figure 5. Comparison of the inner regions of the retina. **A**: Without a fluorescent nuclear dye (ethidium bromide homodimer; EthD-1) counterstain. **B**: With nuclear fluorescent dye. Panels **A** and **B** show the ganglion cell layer imaged with third harmonic generation (THG) and two-photon autofluorescence (TPAF). The EthD-1 nuclear staining (Panel **B**, x), coincides with the THG signal from the ganglion cell nuclei (Panel **A**, *). Panel **C** shows an adjacent histological section stained with hematoxylin and eosin. The scale bar represents 20 µm.

setups that would result in additional layers of complexity and cost.

THG offers an alternative to CARS microscopy for label-free "lipid-specific" imaging since this technique uses a single laser source. THG is a nonlinear scattering phenomenon in which three photons are instantly converted into a single photon three times the energy (Figure 1B). In our experimental setup, for example, a laser with a center wavelength of about 1044 nm generates a THG signal at about 348 nm. Generally, THG can be produced in any media. However, under multiphoton microscopic conditions where high numerical apertures are used to focus the laser beam in the sample, no THG signal is generated in homogenous media with normal dispersion (Figure 1C). Instead, the THG signal is obtained from heterogeneities of size comparable to that of the beam focus; that is, the interfaces between two media (Figure 1D) must fit within the focal volume. The magnitude of the THG signal scales with differences between the third-order nonlinear susceptibility, $\chi^{(3)}$, between the two interfaces. Lipid concentrations inside cellular structures possess optical third-order nonlinear susceptibilities that are distinct from an aqueous environment such as the cell cytoplasm [9,16]. This abrupt change in nonlinear susceptibility in the beam focal volume creates a strong THG signal, a contrast in lipid-specific microscopy. This contrast mechanism makes THG microscopy ideal for imaging cellular and subcellular structures that primarily consist of a water milieu with pockets of lipid-rich organelles of different size and functionality. Under multiphoton microscopic conditions, the relevant sizes can range from as small as a lipid droplet (for metabolic studies), drusen-like structures (disease biomarkers), or entire ocular anatomic structures. In Figure 1E, for example, the THG signal from the cell membrane (*), nuclear membrane (+), and occasional fatty lipid droplets (x) of an OK cell creates a "biomarker" for lipid-specific imaging. Highly absorptive materials are also strong sources of THG. In Figure 1F, the light-absorbing pigment granules of the hfRPE cells create contrast for RPE cell microscopy. In our experimental setup, we found the absorption-induced THG signals from the RPE cells were significantly stronger than the lipid-specific THG. In Figure 2A, for example, the RPE cell layer forms an image through the THG signal from the lipidic nuclear membrane. The green fluorescence of the cytoplasm surrounding the RPE nuclei may result from the TPAF signal from the retinyl esters within the retinosomes [30] in albino animals. In pigmented animals, however, the THG signal from the RPE layer (Figure 2E, +) is formed by pigment granules of the RPE cells. Here, the strong THG signal from the pigment granules overshadows the THG signal (and AF) from retinosomes and other lipidic organelles. Furthermore, in pigmented and non-pigmented animals, the THG signal from the cell nucleus is likely from dense nuclear membranes and tightly wrapped heterochromatin DNA, and the THG signal from the cell membrane originates from lipids within the plasma membrane (Figure 2B–D, *, +, x).

In this manuscript, we showed lipid-specific THG imaging of the entire retina using a custom-built fiber laser system. The choice of wavelength in our laser design is a balance between ocular spectral transmission that attenuates sharply at about 1100 nm [31], reduced damage threshold due to lower absorption of melanin in the RPE at near IR wavelength [32,33], and compatibility with commercial OCT systems and laser technology that are already being used safely for ocular refractive surgery (1030−1064 nm) [34-36]. The data shown in this manuscript are representative images from numerous experiments that yielded reproducible results. Modification of commercially available multiphoton microscopes to include the THG modality could be as simple as inserting an appropriate chromatic filter in the emission path.

Ideal methods for in vivo imaging of disease markers demand noninvasive and label-free data acquisition with high chemical sensitivity and resolution. We believe retinal imaging using lipids as biomarkers has great potential for studies that would permit precise monitoring of disease-specific events such as alteration of neurochemical and metabolic activities. For example, recent studies have shown a direct correlation between chronic oxidative conditions and lipid-rich drusen formation [37-39], the hallmark contributor to the diagnosis of the dry form of age-related macular degeneration (AMD). We believe THG microscopy offers noninvasive, label-free, and dynamic monitoring of living cellular processes at the subcellular level that would allow for real time and high-speed monitoring of the development and progression of AMD.

In general, THG is generated and collected in a forward-detection configuration, which could be difficult to translate to in vivo application. This is similar to any coherent signal generation where the emitted signal travels in the direction of the excitation beam. However, weaker THG can be detected in an epidetection configuration [11,40]. The detected signal is mainly a product of THG photons scattered from the surrounding tissue. In a similar manner, in vivo THG imaging of the retina could be performed by capturing scattered and reflected signals from other structures inside the eye (similar to OCT). We acknowledge that current translation of this technology to in vivo studies requires overcoming some technical hurdles since the maximum permissible exposure (MPE) for ocular safety [41] limits the power that can be delivered to the retina. In our experimental setup with

8 mW of average power for 22 s exposure (the acquisition time per frame), our radiation power is more than five times the American National Standards Institute (ANSI) MPE. However, we did not observe any structural damage in the retina. Instead, the calculated instantaneous peak power on the retina (600 W) was less than the damage threshold for experimental data [42]. Under in vivo conditions, however, where a lower numerical aperture, higher average powers, and longer integration times are prudent, multiple design parameters including laser wavelength, spatial and temporal beam shaping [43], and lower integration times (increasing the thermal average power limit) are necessary. For example, using a 1300-nm laser line instead of 1044 nm will increase the permissible exposure by more than an order of magnitude [44]. At the same time, the emitted THG signal will be shifted into the visible spectrum resulting in less scattering and absorption inside the eye and enhanced quantum efficiency of PMT detectors. However, even as we work toward overcoming current limitations, this technique can be applied to image unfixed intact animal tissues ex vivo. The current work establishes the building blocks of knowledge for in vivo imaging.

## ACKNOWLEDGMENTS

The authors (OM, TLC, MYK and DAA) wish to disclose that they are named as inventors on a patent application for the technology/methodology described in this manuscript. TCL is supported by NIH/NIDDK Grant Number K25DK095232. The work performed in the Department of Ophthalmology is supported by the Slater Family Endowment. OM is partially supported by the donors of the BrightFocus Foundation.

## REFERENCES

1. Huang D, Swanson EA, Lin CP, Schuman JS, Stinson WG, Chang W, Hee MR, Flotte T, Gregory K, Puliafito CA, Fujimoto JG. Optical Coherence Tomography. Science 1991; 254:1178-81. [PMID: 1957169].
2. Swanson EA, Izatt JA, Hee MR, Huang D, Lin CP, Schuman JS, Puliafito CA, Fujimoto JG. In-Vivo Retinal Imaging by Optical Coherence Tomography. Opt Lett 1993; 18:1864-6. [PMID: 19829430].
3. Wojtkowski M, Leitgeb R, Kowalczyk A, Bajraszewski T, Fercher AF. In vivo human retinal imaging by Fourier domain optical coherence tomography. J Biomed Opt 2002; 7:457-63. [PMID: 12175297].
4. Roorda A, Romero-Borja F, Donnelly WJ, Queener H, Hebert TJ, Campbell MCW. Adaptive optics scanning laser ophthalmoscopy. Opt Express 2002; 10:405-12. [PMID: 19436374].
5. Zawadzki RJ, Jones SM, Olivier SS, Zhao MT, Bower BA, Izatt JA, Choi S, Laut S, Werner JS. Adaptive-optics optical coherence tomography for high-resolution and high-speed 3D retinal in vivo imaging. Opt Express 2005; 13:8532-46. [PMID: 19096728].
6. Rossi EA, Chung M, Dubra A, Hunter JJ, Merigan WH, Williams DR. Imaging retinal mosaics in the living eye. Eye (Lond) 2011; 25:301-8. [PMID: 21390064].
7. Barad Y, Eisenberg H, Horowitz M, Silberberg Y. Nonlinear scanning laser microscopy by third harmonic generation. Appl Phys Lett 1997; 70:922-4. .
8. Squier J, Muller M, Brakenhoff GJ, Wilson KR. Third harmonic generation microscopy. Opt Express 1998; 3:315-24. [PMID: 19384376].
9. Débarre D, Supatto W, Pena AM, Fabre A, Tordjmann T, Combettes L, Schanne-Klein MC, Beaurepaire E. Imaging lipid bodies in cells and tissues using third-harmonic generation microscopy. Nat Methods 2006; 3:47-53. [PMID: 16369553].
10. Witte S, Negrean A, Lodder JC, de Kock CPJ, Silva GT, Mansvelder HD, Groot ML. Label-free live brain imaging and targeted patching with third-harmonic generation microscopy. Proc Natl Acad Sci USA 2011; 108:5970-5. [PMID: 21444784].
11. Tserevelakis GJ, Megalou EV, Filippidis G, Petanidou B, Fotakis C, Tavernarakis N. Label-Free Imaging of Lipid Depositions in C. elegans Using Third-Harmonic Generation Microscopy. PLoS ONE 2014; 9:[PMID: 24392137].
12. Zimmerley M, Mahou P, Debarre D, Schanne-Klein MC, Beaurepaire E. Probing Ordered Lipid Assemblies with Polarized Third-Harmonic-Generation Microscopy. Phys Rev 2013; 3:3-.
13. Aptel F, Olivier N, Deniset-Besseau A, Legeais JM, Plamann K, Schanne-Klein MC, Beaurepaire E. Multimodal Nonlinear Imaging of the Human Cornea. Invest Ophthalmol Vis Sci 2010; 51:2459-65. [PMID: 20071677].
14. Denk W, Strickler JH, Webb WW. Two-photon laser scanning fluorescence microscopy. Science 1990; 248:73-6. [PMID: 2321027].
15. Maminishkis A, Chen S, Jalickee S, Banzon T, Shi G, Wang FE, Ehalt T, Hammer JA, Miller SS. Confluent monolayers of cultured human fetal retinal pigment epithelium exhibit morphology and physiology of native tissue. Invest Ophthalmol Vis Sci 2006; 47:3612-24. [PMID: 16877436].
16. Chong A, Buckley J, Renninger W, Wise F. All-normal-dispersion femtosecond fiber laser. Opt Express 2006; 14:10095-100. [PMID: 19529404].
17. Campagnola P. Second harmonic generation imaging microscopy: applications to diseases diagnostics. Anal Chem 2011; 83:3224-31. [PMID: 21446646].
18. Thomas ME, Morrison AR, Schreiner GF. Metabolic effects of fatty acid-bearing albumin on a proximal tubule cell line. Am J Physiol 1995; 268:F1177-84. [PMID: 7611458].
19. Baschong W, Suetterlin R, Laeng RH. Control of autofluorescence of archival formaldehyde-fixed, paraffin-embedded

tissue in confocal laser scanning microscopy (CLSM). J Histochem Cytochem 2001; 49:1565-72. [PMID: 11724904].

20. Rakic B, Sagan SM, Noestheden M, Belanger S, Nan XL, Evans CL, Xie XS, Pezacki JP. Peroxisome proliferator-activated receptor alpha antagonism inhibits hepatitis C virus replication. Chem Biol 2006; 13:23-30. [PMID: 16426968].
21. Tong L, Lu Y, Lee RJ, Cheng JX. Imaging receptor-mediated endocytosis with a polymeric nanoparticle-based coherent anti-stokes raman scattering probe. J Phys Chem B 2007; 111:9980-5. [PMID: 17663581].
22. Kaufman LJ, Brangwynne CP, Kasza KE, Filippidi E, Gordon VD, Deisboeck TS, Weitz DA. Glioma expansion in collagen I matrices: Analyzing collagen concentration-dependent growth and motility patterns. Biophys J 2005; 89:635-50. [PMID: 15849239].
23. Conovaloff A, Wang HW, Cheng JX, Panitch A. Imaging growth of neurites in conditioned hydrogel by coherent anti-Stokes Raman scattering microscopy. Organogenesis 2009; 5:231-7. [PMID: 20539743].
24. Brackmann C, Esguerra M, Olausson D, Delbro D, Krettek A, Gatenholm P, Enejder A. Coherent anti-Stokes Raman scattering microscopy of human smooth muscle cells in bioengineered tissue scaffolds. J Biomed Opt 2011; 16:[PMID: 21361678].
25. Cheng JX, Xie XS. Coherent anti-Stokes Raman scattering microscopy: Instrumentation, theory, and applications. J Phys Chem B 2004; 108:827-40. .
26. Potma EO, de Boeij WP, Wiersma DA. Nonlinear coherent four-wave mixing in optical microscopy. J Opt Soc Am B 2000; 17:1678-84. .
27. Zumbusch A, Holtom GR, Xie XS. Three-dimensional vibrational imaging by coherent anti-Stokes Raman scattering. Phys Rev Lett 1999; 82:4142-5. .
28. Xie XS, Yu J, Yang WY. Perspective - Living cells as test tubes. Science 2006; 312:228-30. [PMID: 16614211].
29. Masihzadeh O, Ammar DA, Kahook MY, Lei TC. Coherent Anti-Stokes Raman Scattering (CARS) Microscopy: A Novel Technique for Imaging the Retina. Invest Ophthalmol Vis Sci 2013; 54:3094-101. [PMID: 23580484].
30. Imanishi Y, Sun WY, Maeda T, Maeda A, Palczewski K. Retinyl ester homeostasis in the adipose differentiation-related protein-deficient retina. J Biol Chem 2008; 283:25091-102. [PMID: 18606814].
31. Boettner EA, Wolter JR. Transmission of the Ocular Media. Invest Ophthalmol Vis Sci 1962; 1:1-.
32. Wang J, Sramek C, Paulus YM, Lavinsky D, Schuele G, Anderson D, Dewey D, Palanker D. Retinal safety of near-infrared lasers in cataract surgery. J Biomed Opt 2012; 17:[PMID: 23085903].
33. Brinkmann R, Huttmann G, Rogener J, Roider J, Birngruber R, Lin CP. Origin of retinal pigment epithelium cell damage by pulsed laser irradiance in the nanosecond to microsecond time regimen. Lasers Surg Med 2000; 27:451-64. [PMID: 11126439].
34. Palanker DV, Blumenkranz MS, Andersen D, Wiltberger M, Marcellino G, Gooding P, Angeley D, Schuele G, Woodley B, Simoneau M, Friedman NJ, Seibel B, Batlle J, Feliz R, Talamo J, Culbertson W. Femtosecond Laser-Assisted Cataract Surgery with Integrated Optical Coherence Tomography. Sci Transl Med 2010; 2:[PMID: 21084720].
35. Friedman NJ, Palanker DV, Schuele G, Andersen D, Marcellino G, Seibel BS, Battle J, Feliz R, Talamo JH, Blumenkranz MS, Culbertson WW. Femtosecond laser capsulotomy. J Cataract Refract Surg 2011; 37:1189-98. [PMID: 21700099].
36. Plamann K, Aptel F, Arnold CL, Courjaud A, Crotti C, Deloison F, Druon F, Georges P, Hanna M, Legeais JM, Morin F, Mottay E, Nuzzo V, Peyrot DA, Savoldelli M. Ultrashort pulse laser surgery of the cornea and the sclera. J Optics-Uk 2010; 12:.
37. Rabin DM, Rabin RL, Blenkinsop TA, Temple S, Stern JH. Chronic oxidative stress upregulates Drusen-related protein expression in adult human RPE stem cell-derived RPE cells: A novel culture model for dry AMD. Aging-Us 2013; 5:51-66. [PMID: 23257616].
38. Bailey TA, Kanuga N, Romero IA, Greenwood J, Luthert PJ, Cheetham ME. Oxidative stress affects the junctional integrity of retinal pigment epithelial cells. Invest Ophthalmol Vis Sci 2004; 45:675-84. [PMID: 14744914].
39. Imamura Y, Noda S, Hashizume K, Shinoda K, Yamaguchi M, Uchiyama S, Shimizu T, Mizushima Y, Shirasawa T, Tsubota K. Drusen, choroidal neovascularization, and retinal pigment epithelium dysfunction in SOD1-deficient mice: A model of age-related macular degeneration. Proc Natl Acad Sci USA 2006; 103:11282-7. [PMID: 16844785].
40. Débarre D, Olivier N, Beaurepaire E. Signal epidetection in third-harmonic generation microscopy of turbid media. Opt Express 2007; 15:8913-24. [PMID: 19547229].
41. Delori FC, Webb RH, Sliney DH. Maximum permissible exposures for ocular safety (ANSI 2000), with emphasis on ophthalmic devices. J Opt Soc Am A Opt Image Sci Vis 2007; 24:1250-65. [PMID: 17429471].
42. Goldman AI, Ham WT, Mueller HA. Mechanisms of Retinal Damage Resulting from Exposure of Rhesus-Monkeys to Ultrashort Laser Pulses. Exp Eye Res 1975; 21:457-69. [PMID: 812713].
43. Block E, Greco M, Vitek D, Masihzadeh O, Ammar DA, Kahook MY, Mandava N, Durfee C, Squier J. Simultaneous spatial and temporal focusing for tissue ablation. Biomed Opt Express 2013; 4:831-41. [PMID: 23761847].
44. Zuclich JA, Gagliano DA, Cheney F, Stuck BE, Zwick H, Edsall PR, Lund DJ. Ocular effects of penetrating IR laser wavelengths. 1995; 1995. p. 112–25.

Articles are provided courtesy of Emory University and the Zhongshan Ophthalmic Center, Sun Yat-sen University, P.R. China. The print version of this article was created on 2 May 2015. This reflects all typographical corrections and errata to the article through that date. Details of any changes may be found in the online version of the article.